

Application of uncertainty visualization methods to meteorological trajectories

Ryan A. Boller · Scott A. Braun · Jadrian Miles · David H. Laidlaw

Received: 31 August 2009 / Accepted: 14 April 2010 / Published online: 18 May 2010
© US Government 2010

Abstract We present an application of uncertainty visualization to air parcel trajectories generated from a global meteorological model. We derive an approximation of advection uncertainty due to interpolation and incorporate this uncertainty into our visualization of trajectories. Our work enables efficient visual pruning of unlikely results, especially in regions of atmospheric shear, potentially reducing erroneous interpretations. Finally, we apply these methods to a real-world meteorological problem to demonstrate its use.

Keywords Uncertainty visualization · Multi-field visualization · Flow visualization · Time-varying data · Meteorological visualization techniques

Introduction

This paper describes an application of uncertainty visualization methods to trajectories in meteorological flow and a novel estimate of uncertainty due to interpolation of discrete flow data. The driving goal of this system is to allow a user to efficiently identify the relative confidence of various trajectories when the data or circumstances are less than ideal, and thereby support a nuanced interpretation of the data. We demonstrate the utility of the system with a pair of use cases in which we investigate the interaction between a hurricane and its local environment. Some

important factors in understanding this interaction are the air's source, path, and composition.

Trajectories begin, or are “seeded,” as a set of particles at a user-specified location in space and time, then follow the local flow through a time-varying vector field. In meteorological studies, this initial volume of seeds is known as an air parcel; the vector field is the air parcel 3-dimensional velocity. To determine the sources that contribute to the composition of a given air parcel, trajectories may be seeded at a chosen final position and propagated backward through time and space, as demonstrated by Chen et al. (2002) and many others. Along the way, one may also maintain “snapshots” in time of each trajectory's properties, such as its relative humidity.

While these analyses provide a good approximation of the air parcels' true paths, the problem of identifying and representing sources of potential uncertainty (Johnson and Sanderson 2003) is often overlooked. The trajectories are a derived quantity, but the various sources of uncertainty in their derivations (Stohl et al. 1995) are rarely represented (Lopes and Brodlie 1998). In contrast, other factors in atmospheric studies, such as humidity, chemical reactions, and chemical dissipation, are routinely modeled with uncertainty and natural variation taken into account; for example, see Bergin et al. (1999). The uncertainty in the trajectories of air parcels themselves would complement such already thorough statistical analysis.

Atmospheric flow fields, whether empirical observations or derived from simulations, are only defined at discrete positions in space and time; at all other positions, the value of the flow field is unknown and must be estimated by interpolating from nearby known values, and therefore some uncertainty is inherent in the interpolation. We provide an approximation and visual representation for the uncertainty of particle trajectories due to interpolation of discretized, time-varying three-dimensional flow field data. The aim is to prevent the user from reaching erroneous conclusions about a meteorological phenomenon based

Communicated by Thomas Narock

R. A. Boller (✉) · S. A. Braun
NASA / Goddard Space Flight Center,
Greenbelt, MD, USA
e-mail: Ryan.A.Boller@nasa.gov

J. Miles · D. H. Laidlaw
Department of Computer Science, Brown University,
Providence, RI, USA

upon trajectories with a high degree of uncertainty resulting, for example, from passage of air parcels through regions of sharp velocity gradients. A user may set a strict threshold to remove trajectories with unacceptably high uncertainty, or may visually prune uncertain results with the aid of the uncertainty visualization.

To demonstrate these techniques in a real-world research scenario, we investigated a meteorological theory (Dunkerton et al. 2008) proposing that hurricanes develop in a “marsupial pouch” of relatively isolated air that travels with the storm. We examined trajectories seeded near developing hurricanes for evidence that this pouch protects the storm’s core from outside influence.

Another case study was to search for sources of dry air that may inhibit hurricane development. The Saharan Desert is one well-studied source of dry air (Karyampudi and Carlson 1988), but the middle latitudes to the north can be another source. We use uncertainty representations to gain a deeper understanding of the underlying data and quickly prune unlikely results.

Related work

This work presents a quantitative approximation of uncertainty in trajectories over time-varying 3D flow fields, discretely sampled in time and space, due exclusively to the arbitrary choice of interpolation between sample points. While the methods and error analysis of numerical integration are well established for analytic differential equations, work on other sources of error (or uncertainty, in the case where the truth is unknown) in trajectory calculations in discrete regimes is relatively recent.

There are three commonly acknowledged sources of uncertainty in the calculation of a trajectory from discrete data: (1) integration error due to the choice of step size (also known as truncation error), (2) the uncertainty of interpolated flow field values, and (3) the intrinsic complexity of the flow system. Truncation error is well studied and may be bounded to an arbitrarily small value by choosing a sufficiently small step size. Many authors have studied the other two sources of uncertainty from diverse perspectives; this work focuses exclusively on interpolation.

Kahl and Samson (1986) and Draxler (1991) conducted empirical studies to characterize the typical distribution of local and aggregate interpolation errors relative to atmospheric observations. Other studies derived reference trajectories from analytic (Shirayama 1993) or high-resolution (Stohl et al. 1995) data, and quantified the deviation from these reference trajectories of trajectories derived from interpolated lower-resolution data. The results of these studies indicate best practices for experiment designers when choosing the spatial and temporal resolu-

tion of their data and an interpolation technique, but do not aid in evaluating the uncertainty of trajectories due to these factors when the resolution is fixed.

In some flow systems, a small change in the position of a seed point results in a large change in the resulting trajectory. This sensitivity (also called “chaos”) is an intrinsic property of the flow system; it would still be present even if the input data had infinite spatial and temporal resolution. Darmofal and Haimes (1996) undertook a thorough study of truncation error and chaotic complexity in analytic flow fields, assuming arbitrary spatial and temporal resolution. Interpolation is unnecessary in such a regime, and so the study did not address interpolation uncertainty.

Kahl (1996) measured trajectory uncertainty in 2-D, time-varying flow fields by comparing “perturbed” trajectories to “reference” trajectories. Each perturbed trajectory was generated by stochastically perturbing the first time step of the flow field with Gaussian noise in each dimension (with standard deviations derived from the empirical studies mentioned above), and then advecting from the seed point according to this modified flow field. Only the first time step was modified; after the first, the flow field was identical for all perturbed trajectories as well as the reference trajectories. This amounts to stochastically perturbing the seed points for an equivalent system starting at the second time step, and so the deviation of the perturbed trajectories from the reference trajectories is due entirely to the chaotic complexity of the system, not interpolation uncertainty.

Another component of the present work is the visualization of trajectory uncertainty. Lopes and Brodlie (1998) formulated a framework for describing sources of error in flow visualization, including interpolation inaccuracy in discrete fields, but did not define a measure for interpolation uncertainty, nor address time-varying fields. The visualization community has developed generic techniques for incorporating local and accumulated uncertainty in visualizations of flow trajectories, such as those by Wittenbrink et al. (1996) and Pang et al. (1997). In the end, we map total trajectory uncertainty inversely to line thickness as described in Section “Visualization” below. Our usage is distinct from prior methods by using this mapping to compare the relative uncertainty of trajectories against others as a collective operation as opposed to looking at trajectories individually.

In selecting a basis for our software development, our system needed to support common data formats, have the ability to simultaneously display multiple meteorological quantities for context, and to provide an interactive 3-D environment so the user can quickly prune problematic results. The Grid Analysis and Display System, GrADS, (Berman et al. 2001) allows input from a variety of data sources, but its trajectory routines are in only two dimensions. Many meteorologists use custom-built trajectory generation software in languages such as IDL, but they

are not publicly available. We required source code access to implement our uncertainty calculations and visualization, which precluded the use of established closed-source packages such as HYSPLIT (Draxler and Rolph 2003) from NOAA and TRAJKS (Scheele et al. 1996) from The Royal Netherlands Meteorological Institute.

Prominent open-source or source-upon-request trajectory generation software for meteorological applications include FLEXTRA (Stohl et al. 1995; Stohl and Seibert 1998) from the Norwegian Institute for Air Research and LAGRANTO (Wernli and Davies 1997) from ETH Zurich. We had previous experience, however, with Unidata’s Java-based Integrated Data Viewer (Murray et al. 2004) and had already used it in preliminary versions of the case study hurricane investigations described below, and so chose to implement our system by modifying IDV. IDV is an open-source package that handles a variety of data formats and coordinate systems, along with providing existing visualization routines that allow our trajectories to be shown in a multi-field context, something that has not been previously implemented as a unified product.

Methods

Trajectory generation

We use a typical method for trajectory generation: fourth-order Runge-Kutta numerical integration, with a fixed step size and linear interpolation over the discrete data. These trajectories can be run forward or backward in time, determining the future or past locations, respectively, of the user-specified seeds.

For testing and validation, we used data produced by global atmospheric analyses from the National Oceanic and Atmospheric Administration’s National Centers for Environmental Prediction. The analyses contain information on atmospheric temperature, pressure, humidity, and 3-dimensional air velocities at six-hour increments with a spatial resolution of 1° latitude by 1° longitude on a pressure coordinate system at 50hPa intervals.

Uncertainty estimation

In a regular spatio-temporal sampling grid, the unit cell is a four-dimensional hypercube, with one sample point at each of its 16 corners (see Fig. 1). While a priori knowledge of fluid flow may indicate that linear interpolation is a better estimate of the velocity within the hypercube than the nearest neighbor, and that quadratic or cubic interpolation are better than linear, the true distribution is unknown. We wish to estimate the variation over an entire trajectory due to possible extreme values of the distribution within each hypercube based on the values at the corners.

Our estimate consists of the assumption that, at any point x in the interior of the hypercube, each component of the true velocity $v(x)$ is bounded by the extreme values of that component in the velocities observed at the surrounding corner points:

$$\hat{v}_i(x) \equiv \{v_i(y) | y \in N(x)\}$$

$$v_i(x) \in [\min(\hat{v}_i(x)), \max(\hat{v}_i(x))]$$

Here, $N(x)$ is the set of corner points of the hypercube containing the point x .

We wish to identify trajectories that deviate from the “main” trajectory that is computed with interpolated velocity values. The maximum deviation within each hypercube results from a constant velocity whose value in each component is one of the extreme values identified by the bound. Therefore, with two choices per component and three components to the velocity vectors, we must test eight different combinations of extreme values to find the trajectory within each hypercube that differs most from the main trajectory. This difference is taken to be an estimate of the local uncertainty in the main trajectory due to interpolation.

Computing the aggregate uncertainty over the course of the entire length of a trajectory requires $O(8^n)$ computations for a trajectory that passes through n hypercubes, since we must consider all extreme directions that the worst-case trajectory could take at every hypercube boundary. Instead we estimate this value in $O(n)$ by considering diverging trajectories of a fixed time length s ; for a main trajectory of time length S , we compute $k = S/s$ diverging trajectories. We estimate the aggregate uncertainty by k multiplied by the maximum distance any diverging trajectory achieves from the main trajectory. Refer to the pseudocode in the Appendix for an algorithmic description of this technique.

This estimate has two clear disadvantages. Firstly, it assumes that the local maxima of all components of the true velocities over the entire space occur exactly at the sampling grid points, which will happen with probability zero. In those cases where a

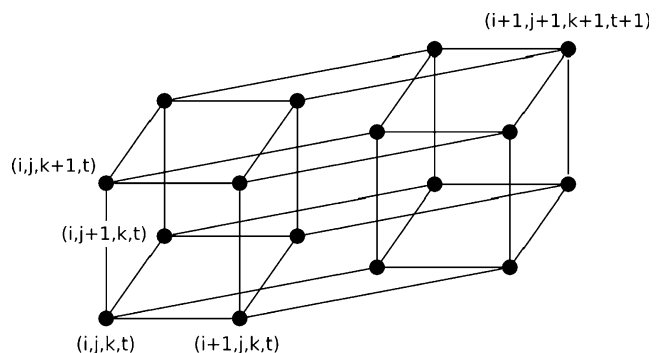


Fig. 1 A cell of the spatio-temporal sampling grid. Sampled velocities are known at each of the corners of the hypercube (black dots), but the value of the distribution within the hypercube is unknown. Certain illustrative sample points are labeled with their sampling indices

true local maximum falls in the interior of a hypercube, it will exceed the assumed bounds described above. For a sufficiently tight sampling grid, however, it is reasonable to assume that the maxima will not exceed the bounds by very much, and a hypercube containing a maximum will be rare relative to the typical case, in which our assumption holds true.

Secondly, the estimated bound is very loose in the typical case. It allows worst-case trajectories to have velocity discontinuities, which are physically impossible. Once again, however, for a sufficiently tight sampling grid, these discontinuities are small relative to the magnitude of the velocities observed at the nearby grid points. Furthermore, this property means that the estimate errs strongly toward overstating uncertainty; in this sense it is a conservative indicator of interpolation uncertainty, as it only claims confidence in a trajectory if the uncertainty is extremely low.

Visualization

We represent the computed uncertainty through the trajectory's thickness: thinner lines are less certain than their thick counterparts. We chose this mapping to allow the more certain lines to visually dominate the scene, while demoting the less certain ones to a less-prominent role. This decision is arbitrary, though, as it can be argued that the reverse mapping is more intuitive since thicker lines could represent a larger possible range of positions for the given trajectory.

It should also be emphasized that this mapping is done on a per-trajectory basis, not per-vertex. Therefore the thickness of each trajectory represents the cumulative uncertainty over its length in order to quickly determine which trajectories are less valid. With relative ease, however, a modification to this mapping could show local variations of uncertainty along a trajectory by modulating its width on a per-vertex basis, allowing the user to directly determine the regions that contribute to uncertainty.

The use of per-trajectory uncertainty mapping enables quick visual identification of which trajectories contain more uncertainty than others. This process can be considered a qualitative one since the initial results are normalized to scale the most uncertain trajectories to a predefined minimum width and the least uncertain ones to a predefined maximum, showing their relative differences. A more quantitative approach has also been implemented through the use of a slider widget that acts as an interactive threshold using the computed uncertainty values.

To better understand the physical makeup of the air parcels over time, the trajectories can be augmented according to user-specified properties. For the purpose of this study, we color each trajectory segment based upon the relative humidity at the point in time it passed through its local space. This enables a series of “snapshots” over time to be displayed in a single frame. Since these visualization structures paint an aggregate

picture of the physical processes over time, more temporal detail can be provided, as necessary. In a manner similar to Sobel et al.'s (2004) particle flurries, we paint only a portion of the trajectories at a given time step. In their case, the main goal is to reduce occlusion, while ours is to provide an indication of the leading edge of each trajectory at that given point in time. This concept is shown in Fig. 2.

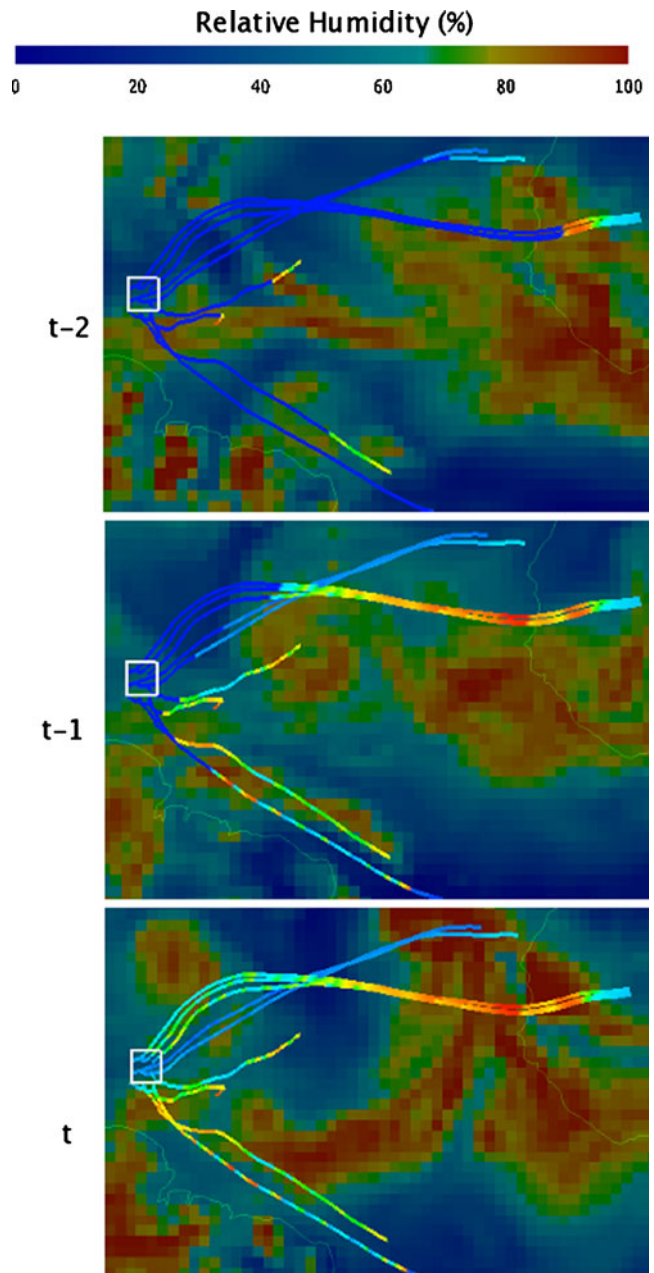


Fig. 2 Underlying, synchronized 2-D color plot shows relative humidity field over time, aiding in understanding the pathlines' context. Pathlines seeded in the white ROI by the user travel back through time; pathline segments are colored according to snapshots of relative humidity; dark blue segments have not yet been “reached” in the currently shown time range

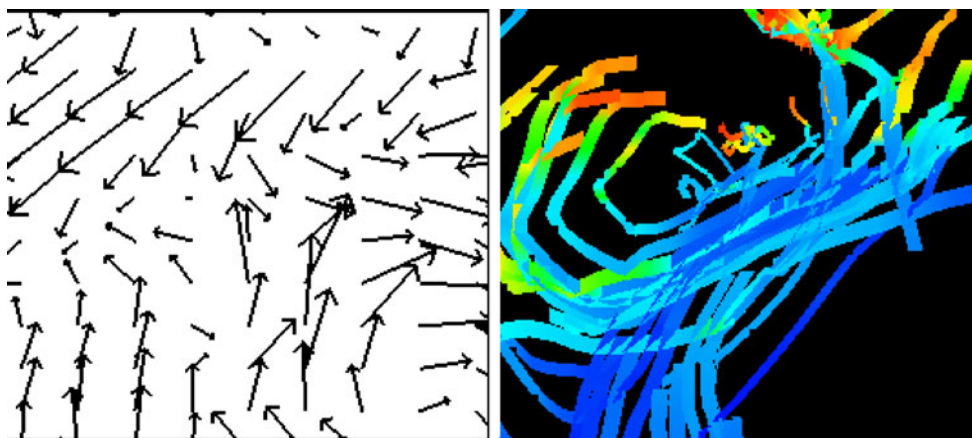


Fig. 3 Using uncertainty to show effects of wind shear on trajectories, facilitating quick visual pruning of unlikely results. *Left*: one time step from the wind field. *Right*: the pathlines of the wind field. Color represents relative humidity “snapshots” as in Fig. 2. Note wind shear at center of field (neighboring vectors in nearly opposite directions)

and its effect on trajectory confidence (thinner lines are less certain). This also eliminates the need to examine the underlying vector field for wind shear at all time steps since each pathline’s uncertainty encompasses the entire range

To aid in the analysis, other meteorological variables (i.e., temperature, pressure) can be viewed simultaneously using a palette of traditional visualization techniques (plan and cross-sectional contour/color plots, isosurface and volume rendering, vector and streamline plots, etc). These plots are synchronized in time with the trajectories’ current position, as shown in Fig. 2. For our case study, it provides a reference frame to the location of the hurricane, aiding in understanding the relationship between air parcel and storm movement.

Results

Visualization and computational results

In the 2-D example shown in Fig. 3, the effects of horizontal wind shear are shown on the trajectories that pass through it. Specifically, this wind shear translates into a greater possible uncertainty of the interpolation used when computing the trajectory vertices in that region. It follows that the trajectories that spend more time in shearing flow accumulate a larger total uncertainty, which is then inversely mapped to its line

thickness. The net result, as shown in Fig. 3, is that the trajectories that travel near the center of the image are less likely to be reliable. As established in the “Methods” section above, our uncertainty estimate overestimates the true uncertainty of the trajectories. However, it does appear to differentiate correctly between high- and low-uncertainty trajectories, and is therefore of practical utility.

As an alternative to proportionally mapping trajectory thickness to its uncertainty, the user may choose to interactively prune the results using a threshold slider widget in the GUI. In this case, all of the trajectories are initialized with a maximum line thickness. As the user adjusts the threshold, the most uncertain trajectories instantaneously change to the minimum line thickness. This provides the ability to quickly locate any patterns of uncertainty, such as clustering of a particularly uncertain set of trajectories. This process is illustrated as a set of images in Fig. 4.

Meteorological results

To address the meteorological question of whether external air systems can affect the developing core of a hurricane,

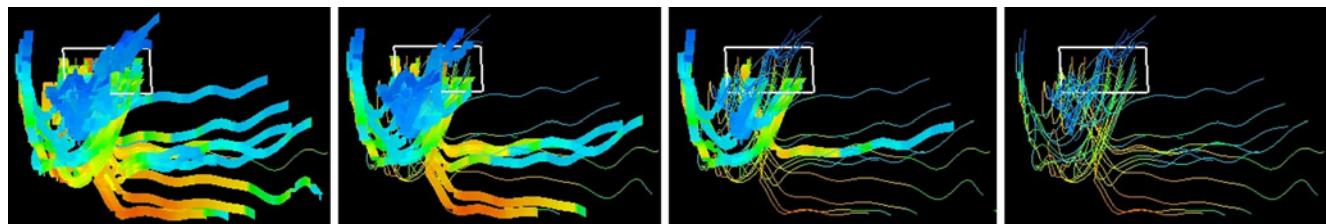


Fig. 4 Interactively adjusting the amount of allowable uncertainty enables the user to quickly discern patterns, such as whether certain trajectory bundles are more reliable than others. Images from left to right show a progressive thresholding of uncertainty values while the most certain trajectories remain thick for the longest amount of time.

In this case, the trajectories on the left part of the images are generally more certain than those on the right. As in previous examples, more certain trajectories are thicker, relative humidity values are mapped to color, and the trajectories are seeded in the white ROI

we generated trajectories from data near hurricanes Isabel (2003), Ivan (2004), and Helene (2006). Our work is still too preliminary to draw scientific conclusions, but it does show some evidence to support the marsupial paradigm.

In Fig. 5, air parcels released near Hurricane Isabel show two distinct groups of trajectories. Trajectories released from dry areas originate from the Sahara and descend from higher, drier levels in the atmosphere. Trajectories released from within the core of the storm originate from lower levels and spiral into the core of the storm from below. The results support the idea of the storm core being protected from the drier surrounding air since no trajectories started within the moist core region come from the drier mid- to upper-level Saharan region. Similar results were obtained for Hurricane Ivan and to an extent, for Helene. However, in Helene, as shown in Fig. 6, a dry air intrusion is seen to extend into the storm from the south and west. The air to the west is found to originate from the east, and likely the

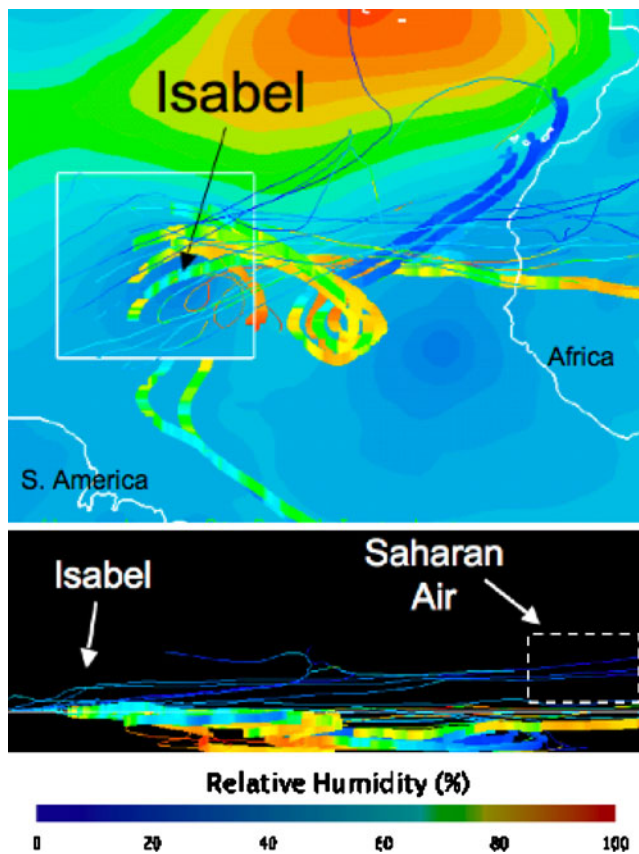


Fig. 5 Overhead and side views of trajectories producing evidence supporting the proposed marsupial paradigm. Air parcels in white box are released around Hurricane Isabel at a height of 700 mb. Dry air (*blue trajectories*) originates above this level and does not enter the interior of the hurricane, while moist air (*warmer-colored trajectories*) originates at lower levels, moves into the storm circulation, and spirals up into the moist region in Isabel. Line thickness indicates path of dry air is generally more uncertain than that of warm air. Background contour plot shows geopotential height (height of pressure surface)

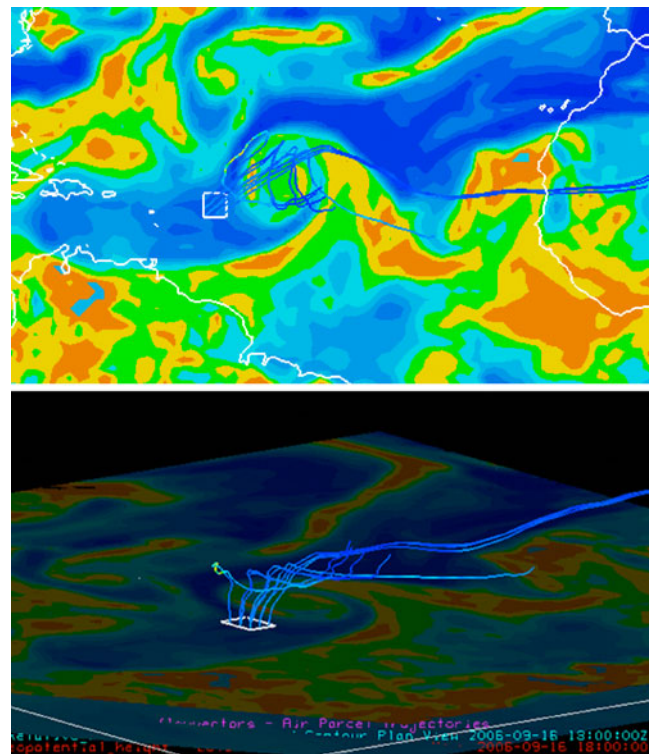


Fig. 6 Overhead and perspective views of dry air, mostly from the Saharan Desert, entering the southwest corner of Hurricane Helene's storm system (*center of top image*) from above. This type of intrusion does not support the marsupial paradigm. Background contour plot shows relative humidity levels

Sahara, but comes from a higher level and descends as the air reaches the western side of the storm. Whether this dry air gets into the inner core of the storm cannot be determined from the coarse-resolution analyses.

When the uncertainty of these trajectories is computed, it paints an unexpected picture. The low-level trajectories pass through the high-gradient regions of the storm while the mid-level trajectories of Saharan origin are moving through the environment where we usually presume the fields to vary far less. As a result, the low-level trajectories should have encountered greater horizontal shear of the wind, but perhaps that is not the case and is something to investigate further.

We then addressed the other meteorological question of looking for sources of dry air not of Saharan origin that might affect hurricane development. In examining data from Helene and Isabel, the search proved to be fruitless, as no sources of dry air from mid-latitudes were found. While this is a preliminary search, it is noteworthy since it reinforces the traditional belief that the Saharan Desert is often the source of dry air.

Conclusions

This work has enabled the efficient generation and analysis of three-dimensional trajectories in a multi-field meteorological

context. We have derived an estimate for the uncertainty of these trajectories due to interpolation error. Using this interpolation error, we have visualized the relative differences in quality between trajectories of a given air parcel, enabling quick visual pruning. We have also demonstrated the application of this work to a real-world meteorological problem.

Acknowledgements The authors wish to thank E.J. Kalafarski/Brown University for implementation of the Runge-Kutta integration algorithm along with Jim Byrnes and the Software Engineering Division at NASA/Goddard Space Flight Center for their support of this research.

Appendix: Pseudocode for uncertainty estimation

```

// Notes:
// * This is example pseudocode intended to illustrate the divergence estimation
//   algorithm. For brevity and clarity, it makes many assumptions and leaves
//   out many details that are carefully addressed in the actual implementation,
//   including:
//   * Assumes time runs forward.
//   * Omits many bounds checks and precision routines.
//   * Measures time in arbitrary units, indicated by T in the comments below,
//     and assumes that the numerical integration timestep and the temporal
//     sampling period of the data are both equal to T.
// * All collections are indexed starting at 0.
// * All variables representing points are 4-D: indices 0-2 are space, 3 is time.
// * A curve is a list of points, one point every T

// elided functions

function get_hypercube(point)
  // returns the hypercube surrounding a given point

function extreme_velocities(hypercube)
  // returns 8 velocities: all combinations of the minimum and maximum
  // velocity component, for each of the 3 space dimensions, found
  // at the 16 corners of the hypercube

function time_to_hypercube_edge(point, hypercube, velocity)
  // returns the time it takes, traveling at the given velocity, to
  // travel from the given point to the edge of the hypercube

function distance(point, point)
  // returns the distance between two points

function interpolate(curve, time)
  // returns the point on the curve at the given time, interpolating
  // between indexed vertices if "time" has a fractional part

function divergence(curve, div_time)
  // div_time is the fixed time length (as a multiple of T) over which to
  // diverge
  max_div = 0 // largest divergence of any diverging trajectory
  for branch_index from 0 to curve.size-1 by div_time
    div_point = curve[branch_index] // first point of diverging trajectory
    while div_point[3] < curve[branch_index][3] + div_time
      hcube = get_hypercube(div_point)
      extreme_velocities = get_extreme_velocities(hcube)
      max_local_div = 0
      div_velocity = [0, 0, 0, 0]
      div_time = 0
      foreach v in extreme_velocities
        t = time_to_hypercube_edge(div_point, hcube, v)
        local_div = distance(
          div_point + v * t,
          interpolate(curve, div_point[3] + t))
        if local_div > max_local_div
          max_local_div = local_div
          div_velocity = v
          div_time = t
        end if
      end foreach
      div_point = div_point + (div_velocity * div_time)
    end while
    max_div = max(
      distance(div_point, interpolate(curve, div_point[3])),
      max_div)
  end for
  return max_div * (curve.size / div_time)

```

References

- Bergin MS, Noblet GS, Petrini K, Dhieux JR, Milford JB, Harley RA (1999) Formal uncertainty analysis of a Lagrangian photochemical air pollution model. *Environ Sci Technol* 33:1116–1126
- Berman F, Chien A, Cooper K, Dongarra J, Foster I, Gannon D, Johnsson L, Kennedy K, Kesselman C, Mellor-Crumme J, Reed D, Torczon L, Wolski R (2001) The GrADS project: software support for high-level grid application development. *Int J High Perform Comput Appl* 15(4):327–344
- Chen LWA, Doddridge BG, Dickerson RR, Chow JC, Henry RC (2002) Origins of fine aerosol mass in the Baltimore-Washington corridor: implications from observation, factor analysis, and ensemble air back trajectories. *Atmos Environ* 36:4541–4554
- Darmofal DL, Haines R (1996) An analysis of 3D particle path integration algorithms. *J Comput Phys* 123(1):182–195
- Draxler RR (1991) The accuracy of trajectories during ANATEX calculated using dynamic model analyses versus rawinsonde observations. *J Appl Meteorol* 30:1446–1467
- Draxler RR, Rolph GD (2003) HYSPLIT (Hybrid Single-Particle Lagrangian Integrated Trajectory) Model access via NOAA ARL READY Website (<http://www.arl.noaa.gov/ready/hysplit4.html>). NOAA Air Resources Laboratory, Silver Spring, MD
- Dunkerton TJ, Montgomery MT, Wang Z (2008) Tropical cyclogenesis in a tropical wave critical layer: easterly waves. *Atmos Chem Phys Discuss* 8:11149–11292
- Johnson CR, Sanderson AR (2003) A next step: visualizing errors and uncertainty. *IEEE Comput Graph Appl* 23(5):6–10
- Kahl JD (1996) On the prediction of trajectory model error. *Atmos Environ* 30(17):2945–2957
- Kahl JD, Samson PJ (1986) Uncertainty in trajectory calculations due to low resolution meteorological data. *J Clim Appl Meteorol* 25:1816–1831
- Karyampudi VM, Carlson TN (1988) Analysis and numerical simulations of the Saharan air layer and its effect on easterly wave disturbances. *J Atmos Sci* 45:3102–3136
- Lopes A, Brodlie K (1998) Accuracy in 3D particle tracing. In: Hege HC, Polthier K (eds) *Mathematical visualization: algorithms, applications and numerics*. Springer Verlag, Heidelberg, pp 329–341
- Murray D, Whittaker T, McWhirter J, Wier S (2004) Integrating GIS data with geoscience data in Unidata's IDV. International conference on interactive information and processing systems for meteorology, oceanography, and hydrology. January 2004
- Pang AT, Wittenbrink CM, Lodha SK (1997) Approaches to uncertainty visualization. *Vis Comput* 13(8):370–390
- Scheele MP, Siegmund PC, Velthoven PFJ (1996) Sensitivity of trajectories to data resolution and its dependence on the starting point: in or outside a tropopause fold. *Meteorol Appl* 3:267–273
- Shirayama S (1993) Processing of computed vector fields for visualization. *J Comput Phys* 106:30–41
- Sobel JS, Forsberg AS, Laidlaw DH, Zeleznik RC, Keefe DF, Pivkin I, Kamiadakis GE, Richardson P, Swartz S (2004) Particle flurries: synoptic 3D pulsatile flow visualization. *IEEE Comput Graph Appl* 24(2):76–85
- Stohl A, Seibert P (1998) Accuracy of trajectories as determined from the conservation of meteorological tracers. *Q J Roy Meteorol Soc* 124:1465–1484
- Stohl A, Wotawa G, Seibert P, Kromp-Kolb H (1995) Interpolation errors in wind fields as a function of spatial and temporal resolution and their impact on different types of kinematic trajectories. *J Appl Meteorol* 34:2149–2165
- Wernli H, Davies HC (1997) A Lagrangian-based analysis of extratropical cyclones. I: The method and some applications. *Q J Roy Meteorol Soc* 123:467–489
- Wittenbrink CM, Pang A, Lodha SK (1996) Glyphs for visualizing uncertainty in vector fields. *IEEE Trans Vis Comput Graph* 2(3):266–279